$\tau \to \pi\pi^0\nu$ event reconstruction and measurement of branching ratio

Zuzana Gruberova, Charles University, Czech Republic

September 4, 2019

Supervisors: Ilya Komarov, Armine Rostomyan, Francesco Tenchini, Petar Rados

Abstract

This note reviews the summer project on $\tau \to \pi\pi^0\nu$ branching ratio measurement for detector performance study. We analyzed data from Belle II experiment using Monte Carlo simulations. We optimized the selections to get a pure sample and calculated the branching ratio, $\mathcal{BR}(\tau \to \pi\pi^0\nu) = (24.5 \pm 0.5)\%$. Only statistical uncertainties were taken into account. Despite this fact, agreement with PDG value is good. We used results of related projects to calculate ratios of branching ratios.

Contents

List of Figures

List of Tables

1. Introduction

Particle experiment Belle II, developed at High Energy Accelerator Research Organisation (KEK) in Tsukuba, Japan, is operated on SuperKEKB accelerator, a 3 km circumference asymmetric e^+e^- collider with $\sqrt{s} = 10.58\text{GeV}$. It is an extension of the previous experiment Belle, which run on KEKB accelerator until 2010. Belle II is a B-factory, it aims at producing large amount of B mesons, but also D mesons and τ pairs for precision measurements.

SuperKEKB is expected to reach the instantaneous luminosity of $8 \times 10^35\ \text{cm}^{-2}\text{s}^{-1}$ and total integrated luminosity of 50 ab^{-1} in 2020's, the Belle II detector is designed to record data with performance similar or better than in Belle in a much more severe beam background environment. [1]

One of the studies performed on Belle II data focuses on properties of τ leptons, the heaviest known leptons. The precision measurements of τ decays can provide an insight into such problems as CP violation, lepton flavour violation or lepton universality. Due to their mass, τ leptons can also decay hadronically, which allows us to study strong interactions as well.

This note presents a study of $\tau \to \pi\pi^0\nu$ event reconstruction using Monte Carlo simulations and measurement of the branching ratio of this decay. This project is one of the four projects on similar topics:

- $\tau \to e\nu\nu$
- $\tau \to \pi\nu$ / $\mu\nu\nu$
- $\tau \to \pi\pi^0\nu$
- $\tau \to 3\pi\nu$

The final parts of this note incorporate output from the other three projects.

2. Theory

Most of the elementary particles are not stable and decay via the weak interaction. One type of a particle can decay in different ways and produce different new particles. The probability of a particle decaying in certain way is characterized by a branching ratio.

Data analysed during this project were collected at the Belle II detector, this section gives a brief overview of the Belle II subdetectors and describes the decay modes of τ lepton with focus on the $\tau \to \pi\pi^0\nu$ decay, how to recognize this event and how to determine the branching ratio.

2.1. Belle II detector

SuperKEKB collides electrons with positrons, where positrons circulate in the Low Energy Ring (LER) of the accelerator at the energy of 4 GeV and electrons travel the opposite direction in the High Energy Ring (HER) at 7 GeV. When two bunches collide, the centre of mass moves in the direction of the electron beam. Therefore, most of the interaction products are detected in the forward direction and thus the layout of the detector is asymmetric. 3D model of the Belle II detector is shown in Figure 2.1.

The tracking system comprises the Pixel Detector (PXD), Strip Vertex Detector (SVD), and the Central Drift Chamber (CDC). The Time Of Propagation counters (TOP) and Aerogel Ring-Imaging Cherenkov detector counters (ARICH) are responsible for particle identification. Crystals of the Electromagnetic Calorimeter (ECL) detect neutral particles and measure the energy of electromagnetically interacting particles. The K_L and muon detector (KLM) surrounds the whole system and detects muons and kaons. [2]

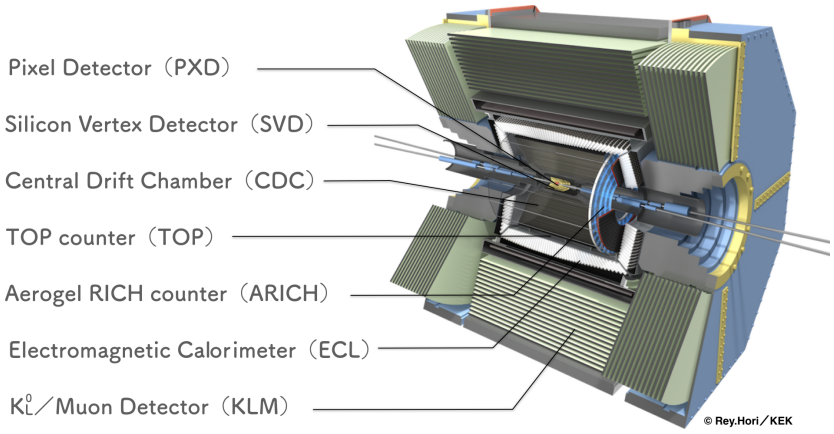

Figure 2.1: *Belle II detector.* The figure shows major Belle II subdetectors. The forward side of Belle II is to the right in the picture. [3]

2.2. τ lepton decay modes

τ leptons are the heaviest of known leptons with mass (1776.86 ± 0.12) MeV and lifetime $(2.903 \pm 0.005) \times 10^{-13}$ s. Therefore, they can decay both leptonically and hadronically. Table 2.1 lists the most dominant decay modes with their branching ratios. In total, τ leptons decay mostly hadronically, and leptonically only in around 35 %.

The decay studied in this note is the most common one. Figure 2.2 shows the Feynman diagram of the $\tau \to \pi\pi^0\nu$ with the intermediate resonance ρ. Other resonances yielding $\pi\pi^0\nu$ are negligibly rare. [4]

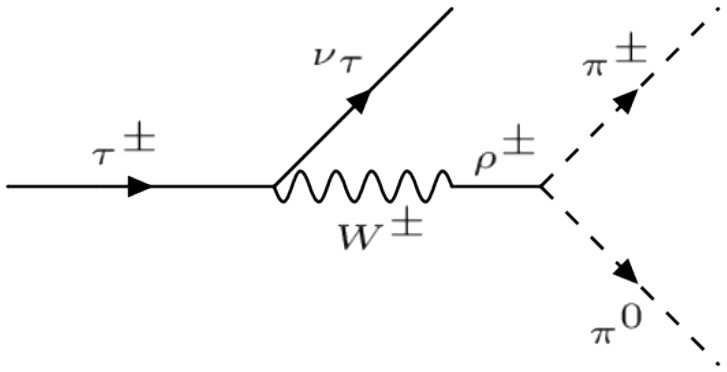

Figure 2.2: *Feynman diagram of* $\tau \to \pi\pi^0\nu$ *decay.* The picture shows the ρ resonance, which is the major intermediate resonance for this decay.

decay mode	branching ratio
$\tau \to \pi\pi^0\nu$	$(25.49 \pm 0.09)\%$
$\tau \to \pi\ nu$	$(10.82 \pm 0.05)\%$
$\tau \to \pi 2\pi^0\nu$	$(9.26 \pm 0.10)\%$
$\tau \to 3\pi\nu$	$(8.99 \pm 0.05)\%$
$\tau \to 3\pi\pi^0\nu$	$(2.74 \pm 0.07)\%$
$\tau \to \pi 3\pi^0\nu$	$(1.04 \pm 0.07)\%$
$\tau \to e\nu\nu$	$(17.82 \pm 0.04)\%$
$\tau \to \mu\nu\nu$	$(17.39 \pm 0.04)\%$

Table 2.1: τ *lepton decay modes.* The complete list of decay modes can be found in [4].

2.3. Event characteristics

τ decays in Belle II detector are always observed in pairs, since collisions of e^+ and e^- always produce a pair of τ leptons, τ^+ and τ^-. We are looking for such events, where one τ decays to $\pi\pi^0\nu$, which is our signal, the other τ to something else, which is the tag process.

$\tau \to \pi\pi^0\nu$ decay produces one charged pion, a π^0, which decays almost immediately to two photons, and a neutrino, which we observe as a missing energy in the event. This kind of decay is called 1-prong decay because we only have one charged particle produced. Our tag side is any 3-prong decay so in total the event contains four charged particles.

τ pair production events are typically back-to-back, which means that the created τ leptons are emitted in opposite directions in the center of mass system. This allows us to divide the space into two hemispheres with respect to the two τ leptons, see Figure 2.3.

The axis, which corresponds to the maximal momentum projection of all visible particles,

is called the thrust axis. We define *thrust value* as follows

$$\text{thrust value} \overset{\max}{=} \sum_i \frac{|\vec{P}_i \cdot \hat{T}|}{|P_i|}, \tag{1}$$

where P_i is the 4-momentum of the particle and $\hat{T}$ is the unit vector in the direction of the thrust axis. Because of the back-to-back property, thrust value is going to be high, close to 1.

On the other hand, visible energy of the event, defined as

$$\text{visible energy} = \sum_i E_i, \tag{2}$$

where E_i is the energy of a visible particle, is going to be less than $E_{CMS}/2 = 5.28$ due to missing neutrinos.

These characteristics will help us in the event reconstruction procedure. [5]

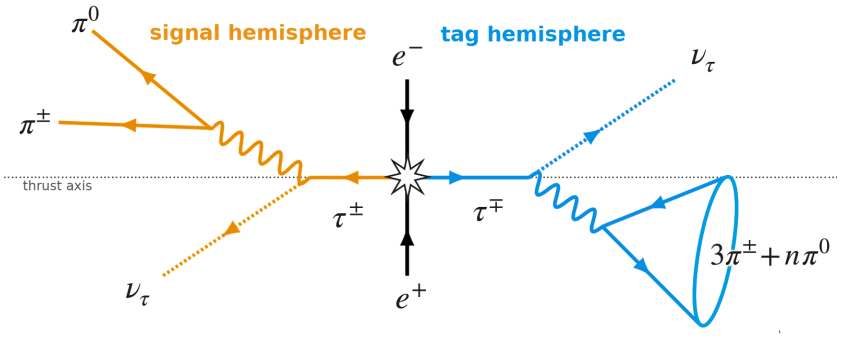

Figure 2.3: *Diagram of the signal event.* On signal side there is the $\tau \to \pi\pi^0\nu$ decay, the tag side is any 3-prong decay.

2.4. Branching ratio

Branching ratio, or branching fraction, of a decay determine the probability of that particular decay. Branching ratio can be measured from data using the following formula

$$\mathcal{BR}_{sig} = \frac{N_{sig}^{data}}{2 \cdot \sigma \cdot \mathcal{BR}_{tag} \cdot \mathcal{L} \cdot \epsilon_{all}}, \tag{3}$$

where N_{sig}^{data} is the number of signal events in data, σ is the cross-section of the studied process, $\mathcal{BR}_{tag}$ is the branching-ratio of the tag process and $\mathcal{L}$ is the integrated luminosity of the experiment. The ϵ_{all} represent all measurement inefficiencies, e. g. the trigger efficiency, efficiencies of different subdetectors, detector acceptance and also efficiency of the selections and cuts applied during the data processing. [5]

The measurement of the branching ratio is also influenced by both statistical and systematic errors of the input variables.

To reduce some of the inefficiencies, and some of the uncertainties, too, one can calculate a ratio of two branching ratios. This was done combining the results of the four projects.

3. Data sets

The following sections describe the experimental data processing, as well as the Monte Carlo simulation characteristics.

3.1. Experimental data

For our analysis we used data collected from March to July 2019 (Proc9), Phase 3, separately Experiment 7 and Experiment 8. These two experiments mark the start of the full detector operation. Integrated luminosity of Exp7, and Exp8 are

$$\mathcal{L}_{Exp7} = (642.8 \pm 3.5)\ \text{pb}^{-1}, \quad \mathcal{L}_{Exp8} = (1982.3 \pm 0.6 \pm 3.5)\ \text{pb}^{-1}.$$

We analyzed the Experiment 7 and 8 independently; for the study we used Exp8, mainly because of higher statistics and because of better behaviour for all the four projects, Exp7 was used as a reference.

3.2. Candidate event selection

To identify candidates for events we are looking for, we require the events to satisfy a number of conditions.

- 4 tracks - 1 track in one hemisphere and 3 tracks in the other hemisphere,
- π^0 reconstruction - for both sides we reconstruct π^0s from photons with energy $>$ 100 MeV, the mass window for π^0s is 0.115 GeV $< m <$ 0.152 GeV,
- additional photons - for both sides we allow reconstruction of additional photons only with energies $>$ 200 MeV to suppress background,
- track selection - all tracks are required to be with the region of $dr < 2$ cm and $dz < 5$ cm, again to suppress background,
- e and μ/π separation - we use `clusterE/p` variable, which is E/p of a cluster of energy deposited in ECL, to distinguish electrons from muons and pions. Electrons are light particles, at GeV energies highly relativistic and the shower is fully contained by the ECL so the energy measument is very accurate. We require `clusterE/p` > 0.8 for e, `clusterE/p` < 0.8 for μ/π. Due to this requirement we also need each track to have an associated ECL hit.

These requirements are the preselection of our data, further restrictions were to be set using Monte Carlo datasets.

3.3. Monte Carlo

To determine the background of our process and adjust further signal selections, we used Monte Carlo simulated data MC12 BGx1 samples for signal and background. Simulated processes are shown in Table 3.1. In all plots, MC components are weighted according to their effective luminosity

$$\mathcal{L}_{eff} = \frac{N}{\sigma}, \tag{4}$$

where N is the number of generated events and σ is the cross-section of the process.

process	name	N [10^6]	cross-section [nb]	1/(luminosity [10^6/nb])
$e^+e^- \to \tau^+\tau^-$	`'tautau'`	73.52	0.919	0.012500
$e^+e^- \to u\bar{u}$	`'uubar'`	128.40	1.61	0.012539
$e^+e^- \to d\bar{d}$	`'ddbar'`	32.08	0.4	0.012469
$e^+e^- \to s\bar{s}$	`'ssbar'`	30.64	0.38	0.012402
$e^+e^- \to c\bar{c}$	`'ccbar'`	106.32	1.3	0.012227
$e^+e^- \to e^+e^-\mu^+\mu^-$	`'eemumu'`	100	18.9	0.189000
$e^+e^- \to \mu^+\mu^-$	`'mumu'`	55	1.148	0.020873
$e^+e^- \to \pi^+\pi^-$	`'pipi'`	200	0.16759	0.000838
$e^+e^- \to e^+e^-\gamma$	`'ee'`	50	300	6.000000
$e^+e^- \to e^+e^-e^+e^-$	`'eeee'`	210.6	39.7	0.188509

Table 3.1: *Simulated processes.* `tautau` is the τ pair event, `uubar, ddbar, ssbar` and `ccbar` are quark pair production backgrounds, `ee` is a radiative Bhabha scattering background, `eeee` and `eemumu` are photon fusion processes, `mum` and `pipi` are other pair production processes. The last column represent the weight of the MC component.

4. Signal selection

Signal selection for the $\pi\pi^0\nu$ samples was done using MCMode match, where MCMode is a variable characterizing the decay mode of the simulated τ. $\pi\pi^0\nu$ signal is MCMode = 4, complete list of τ decay modes can be found in the Attachments. This selection divides simulated τ pair events into `signal` and `tautau_bkg`.

Further in this section, we describe additional cut and trigger selections.

4.1. Cut performance

During data analysis, we cut on different variables in order to get more pure sample. As mentioned in Section 2.2, we expect certain behaviour of signal thrust and visible energy which then enables us to distinguish it form backgrounds.

To characterize cut performance, we define *signal purity* as number of signal events over number of all events,

$$\text{signal purity} = \frac{N_{sig}}{N_{sig} + N_{bkg}}, \tag{5}$$

and *signal efficiency*

$$\text{signal efficiency} = \frac{N_{sig}^{rec}}{2\mathcal{BR}_{sig}\mathcal{BR}_{tag}N_{tot}^{gen}}, \tag{6}$$

where N_{sig}^{rec} is the number of reconstructed signal events, $\mathcal{BR}_{sig}$, resp. $\mathcal{BR}_{tag}$ is the branching ratio of signal, resp. tag process and N_{tot}^{gen} is the total number of generated events.

variable	cut value
`nPi0s_1prong`	`== 1`
`nPhotons_1prong`	`== 0`
`visibleEnergyOfEventCMS`	< 9
`thrust`	> 0.9

Table 4.1: *Cut values.* Cut on the number of π^0s is applied during the preselection.

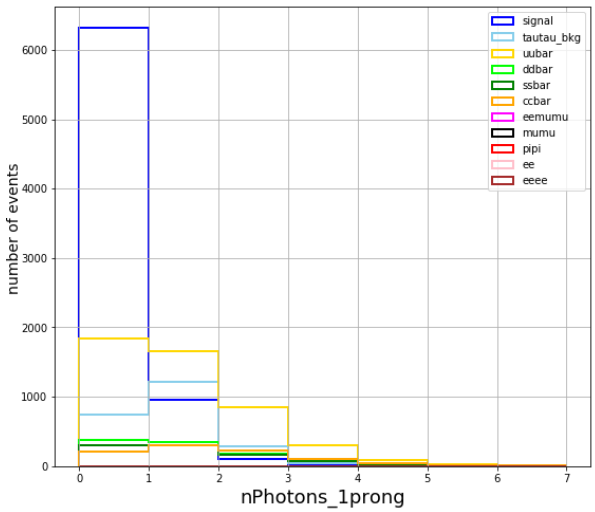

Figure 4.1: *Distribution of number of photons on 1-prong side after preselection.* No additional cuts applied. MC components are not stacked.

4.2. Cut selections

Figures 4.1 and 4.2 show MC components after preselections mentioned in Section 3.3. Table 4.1 lists the cut values.

Our channel selection implicitly means that the number of π^0s on 1-prong side has to be equal to 1.

Next we cut on the number of photons on 1-prong side. In Figure 4.1 we can see that the signal is mostly in the 0 bin, other bins are dominated by backgrounds, this multiplicity cut affects all kinds of background.

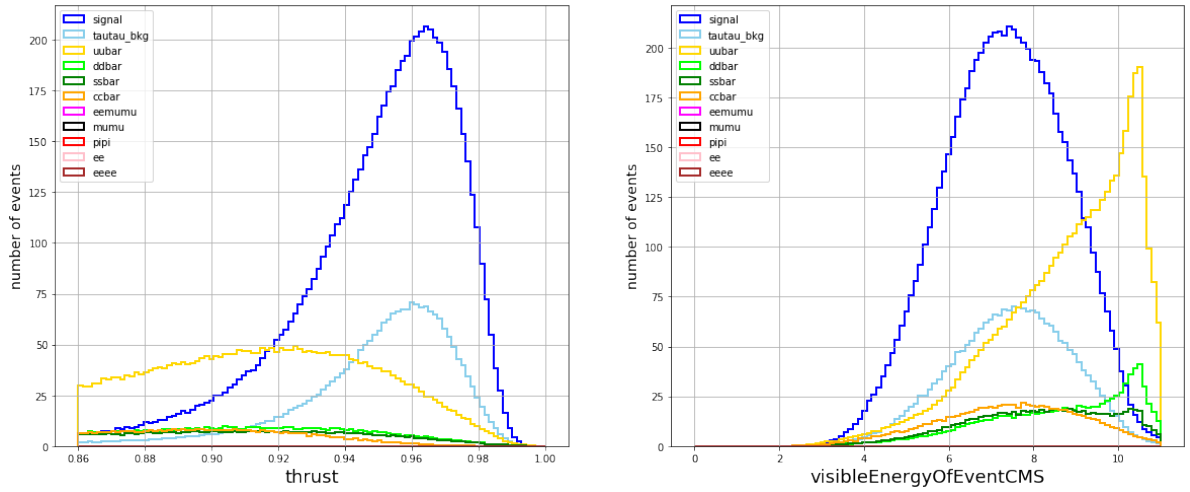

Figure 4.2: *Thrust and visible energy distribution after preselection.* No additional cuts applied. MC components are not stacked.

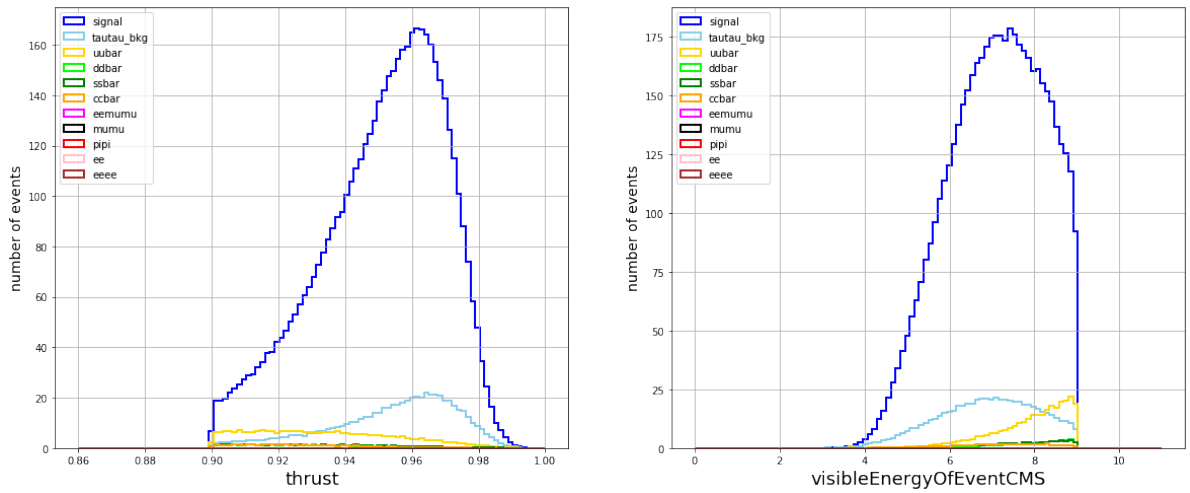

Figure 4.3: *Thrust and visible energy distribution after cuts.* MC components are not stacked.

The cut on visible energy removes the unwanted peak of $q\bar{q}$ background, the cut on thrust then eliminates the tail of thrust distribution, which is also mostly background. Plots showing thrust and visible energy after each cut can be found in the Attachments.

Cut values were optimized by hand with respect to the signal purity. The final values are round because finer tuning has not improved the result. Table of cut efficiencies can be found in the Attachments.

Figure 4.3 show the final MC distributions. The final purity is (82.8 ± 1.6) % with signal efficiency (7.27 ± 0.04) %.

4.3. Trigger

With respect to the preselection, we used two triggers,

- CDC trigger - N of 2D track is >= 3 (output trigger bit fff),
- ECL trigger - ECL total energy > 1 GeV and no Bhabha veto (output trigger bit hie),

where Bhabha event is the $e^+e^- \to e^+e^-$ scattering. This process has a high branching ratio so the energy requirement itself is not sufficient to prevent congestion by this background. Trigger bits are logical statements used to decide whether the event should be read out and stored.

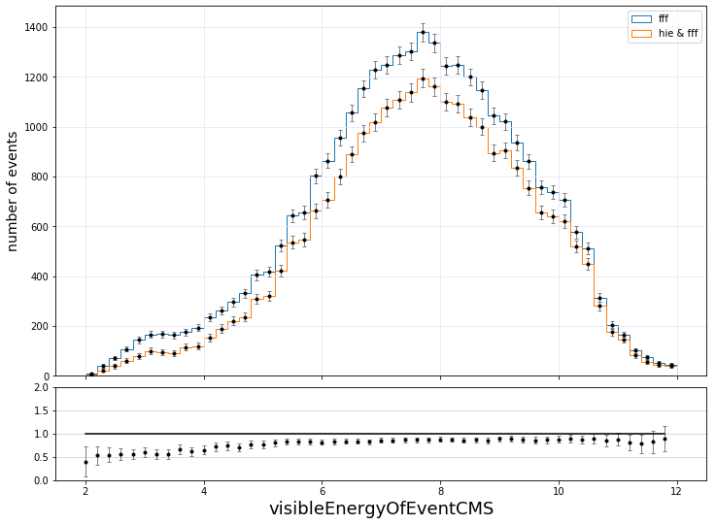

Figure 4.4: *ECL trigger efficiency dependence on visible energy.* The plot shows Exp8 data with both triggers fired and with only reference trigger fired. The ratio plot below is the trigger efficiency

Trigger efficiency is defined as a ratio of number of signal events with the trigger fired and number of all signal events. However, this approach cannot be used since we do not have the number of all signal events, so we use an independent trigger as a reference

trigger. CDC and ECL are orthogonal, which means they are independently activated. The efficiency formula is then

$$\epsilon_{trig}^{hie} = \frac{fff \wedge hie}{fff}, \quad \epsilon_{trig}^{fff} = \frac{fff \wedge hie}{hie}, \tag{7}$$

which is the number of signal events with both triggers fired over the number of events with only the reference trigger fired.

Figures 4.4 and 4.5 show the ECL trigger efficiency dependence on thrust and energy, the error is Poisson statistical error. We used these dependencies to scale down the Monte Carlo histograms in a bin-by-bin matter.

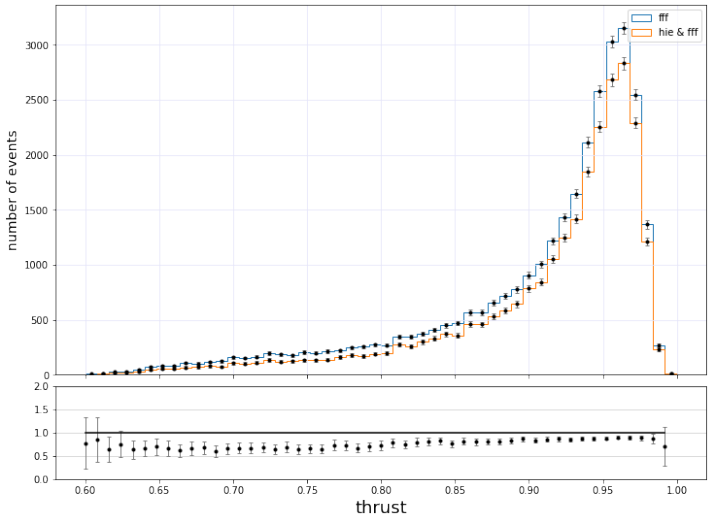

Figure 4.5: *ECL trigger efficiency depnedence on thrust.* The plot shows Exp8 data with both triggers fired and with only reference trigger fired. The ratio plot below is the trigger efficiency

5. Data and Monte Carlo comparison

To get an insight on how background in real data looks, we compared Monte Carlo simulation with measured data.

Before comparing, MC has to be scaled up to the luminosity of experimental data and also scaled down by the trigger efficiency in bin-by-bin manner.

This section shows the comparison plots for different variables.

5.1. Plots

In Figures 5.1 and 5.2 we can see how Exp8 data and MC look after the preselection, without any additional cuts.

After applying all cuts, we get a very good agreement, see Figures 5.3 and 5.4 for Exp8 and Figures 5.5 and 5.6 for Exp7. Plots of thrust and visible energy after each cut for Exp8 are in the Attachments.

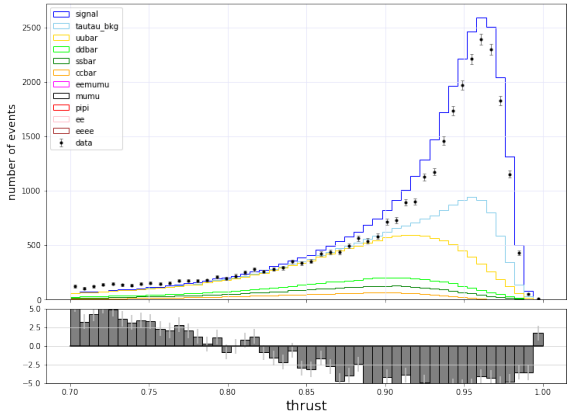

Figure 5.1: *Exp8 data and MC comparison - thrust after preselection.* No additional cuts applied. MC components are stacked.

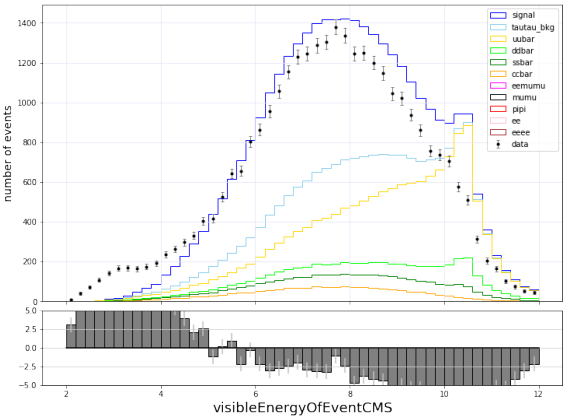

Figure 5.2: *Exp8 data and MC comparison - visible energy after preselection.* No additional cuts applied. MC components are stacked.

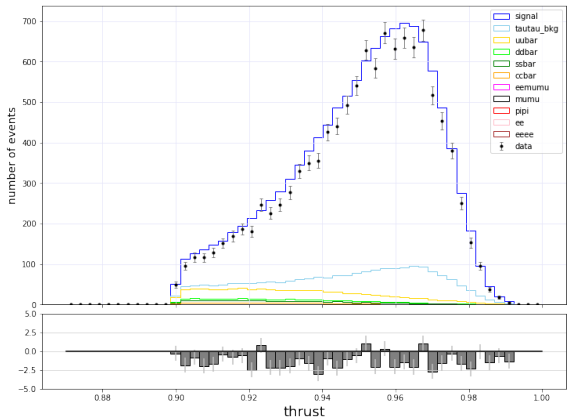

Figure 5.3: *Exp8 data and MC comparison - thrust after cuts.* MC components are stacked.

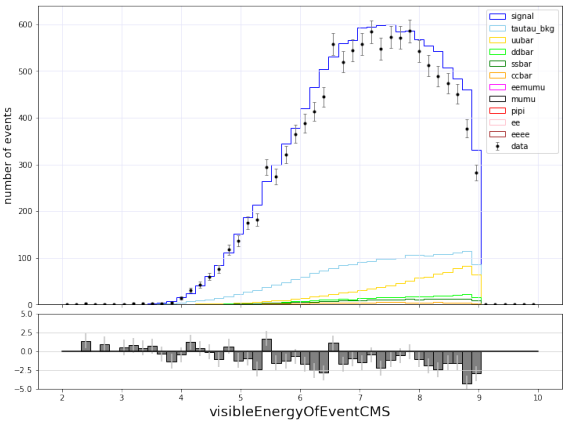

Figure 5.4: *Exp8 data and MC comparison - visible energy after cuts.* MC components are stacked.

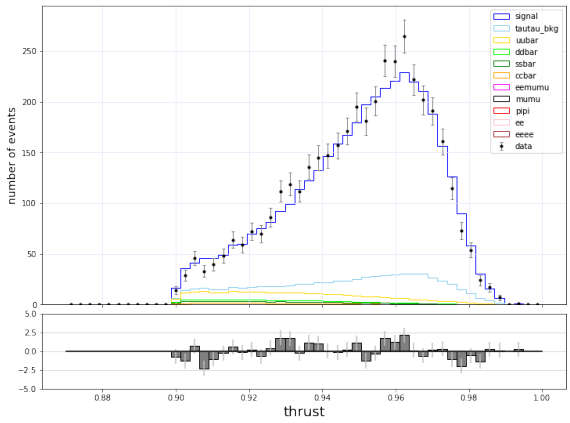

Figure 5.5: *Exp7 data and MC comparison - thrust after cuts.* MC components are stacked.

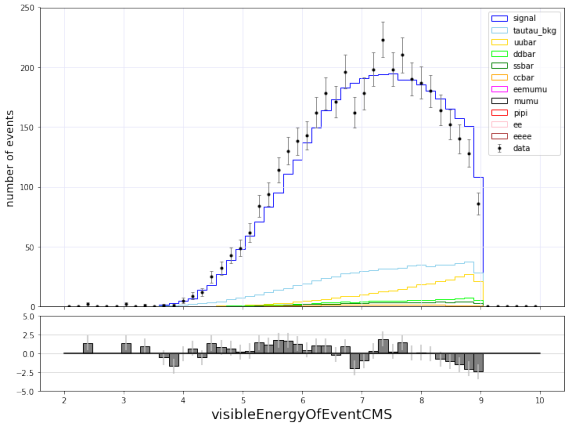

Figure 5.6: *Exp7 data and MC comparison - thrust after cuts.* MC components are stacked.

Plots of other variables show only Exp8 data, corresponding plots for Exp7 can be found in the Attachments.

In Figure 5.7 there is the τ 1-prong invariant mass distribution, we can see that the neutrinos in our events carry away a lot of energy.

Figures 5.8 and 5.9 show π^0 variables, invariant mass and energy. The discrepancy between data and MC here is most likely caused by the difference in π^0 reconstruction in data and MC, which is a consequence of differences in background simulation and has to be further studied. The charged pion energy distribution is plotted in Figure 5.10.

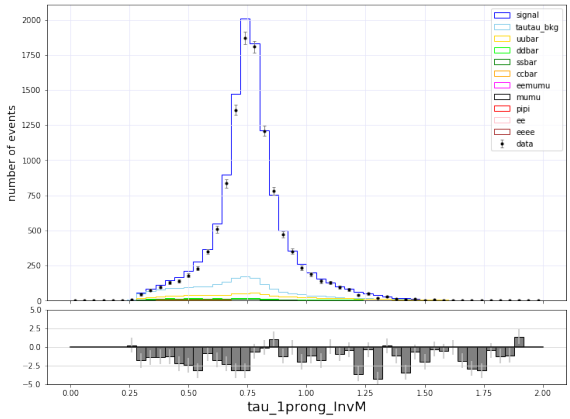

Figure 5.7: *Exp8 data and MC comparison - τ 1-prong invariant mass after cuts.* MC components are stacked.

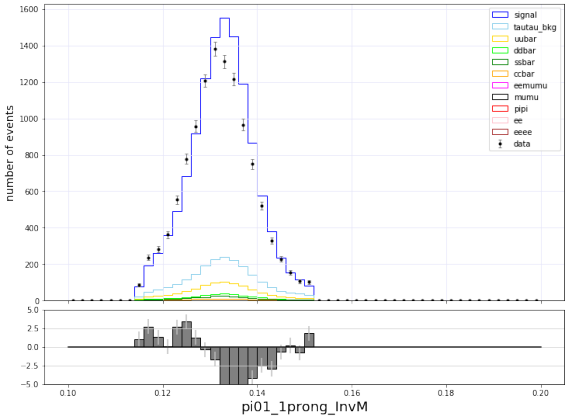

Figure 5.8: *Exp8 data and MC comparison - π^0 1-prong invariant mass after cuts.* MC components are stacked.

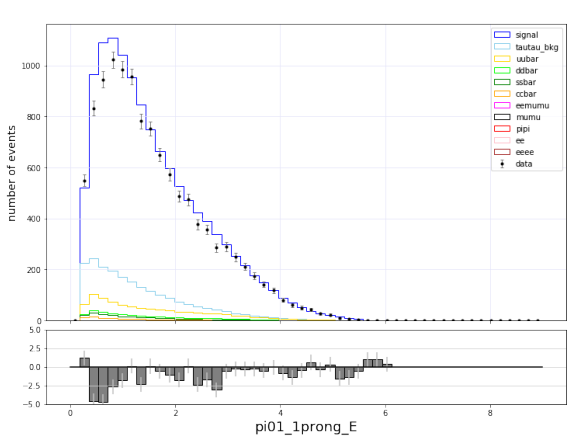

Figure 5.9: *Exp8 data and MC comparison - 1-prong π^0 energy after cuts.* MC components are stacked.

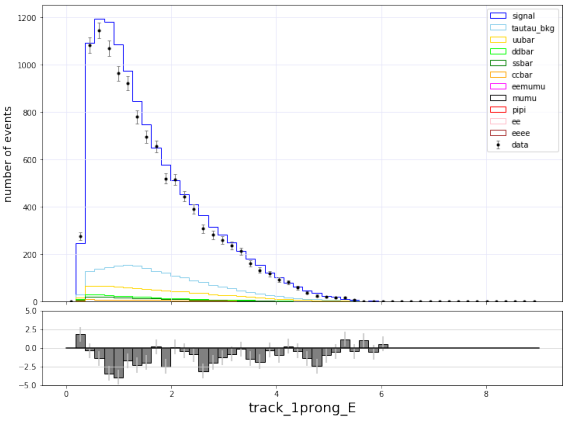

Figure 5.10: *Exp8 data and MC comparison - 1-prong π^0 energy after cuts.* MC components are stacked.

In Figure 5.11 there is the MCMode distribution of 1-prong side Monte Carlo events after all cuts. The most contributing backgrounds come from the a_1 resonance (MCMode 5) and K^* (MCMode 7), which decayed into $KK^0\pi^0$. In both cases we are getting signal from a different event where one or more pi^0s were not reconstructed, in the second case, a kaon is also misidentified as pion.

Apart from the π^0 reconstruction, the agreement between the data and Monte Carlo is very good in all plots.

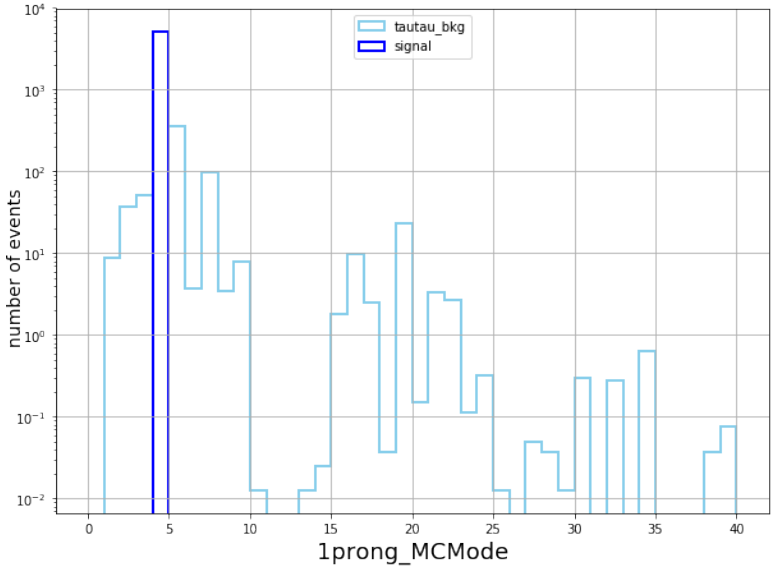

Figure 5.11: *1-prong MCMode distribution after cuts.* The y-axis is logarithmic, we can see that the largest backgrounds are a_1 (MCMode 5) and K^* (MCMode 7).

6. Branching ratio

Using the Formula 3, we can now calculate the branching ratio. In our case, ϵ_{all} consists of the ECL trigger efficiency ϵ_{trig}^{hie} calculated from data for both Exp7 and Exp8, and signal efficiency ϵ_{sig}, which contains the cut efficiency, reconstruction efficiency, tracking efficiency and detector acceptance and was calculated using purely Monte Carlo. Our formula is therefore

$$\mathcal{BR}_{sig} = \frac{N_{sig}^{data}}{2 \cdot \sigma \cdot \mathcal{BR}_{tag} \cdot \mathcal{L} \cdot \epsilon_{trig}^{hie} \cdot \epsilon_{sig}}, \tag{8}$$

where we propagate the statistical errors of $N_{sig}^{data}, \epsilon_{trig}^{hie}$ and ϵ_{sig}. N_{sig}^{data} was calculated from data using MC in the following way

$$N_{sig}^{data} = N^{data} \cdot (\text{signal purity}), \tag{9}$$

where we assume the same error for data and MC. No systematic uncertainties were taken into account.

In this section, we show the branching ratio for $\pi\pi^0\nu$ channel and briefly summarize the combined results from all four projects.

6.1. $\pi\pi^0$ sample

For $\tau \to \pi\pi^0\nu$ channel we list all the variables and their uncertainities (if propagated into the result) used in the branching ratio formula:

- $N^{data} = 11757 \pm 108$
- signal purity $= 0.828 \pm 0.016$
- $\sigma = 0.191$ nb
- $\mathcal{L} = 1.9823$ nb^{-1}
- $\epsilon_{trig}^{hie} = 0.98 \pm 0.02$
- $\epsilon_{sig} = 0.0727 \pm 0.0004$

The branching ratio is

$$\mathcal{BR}_{\tau \to \pi\pi^0\nu} = (24.5 \pm 0.5)\%.$$

PDG value is $(25.49 \pm 0.09)\%$.

6.2. Combined results

To calculate the ratios of branching ratios for τ decays the four projects were combined. Table 6.1 and Figure 6.1 show the calculated branching ratios with corresponding PDG values. For more details about processing the other samples, as well as the PID cut variants, please refer to their individual studies.

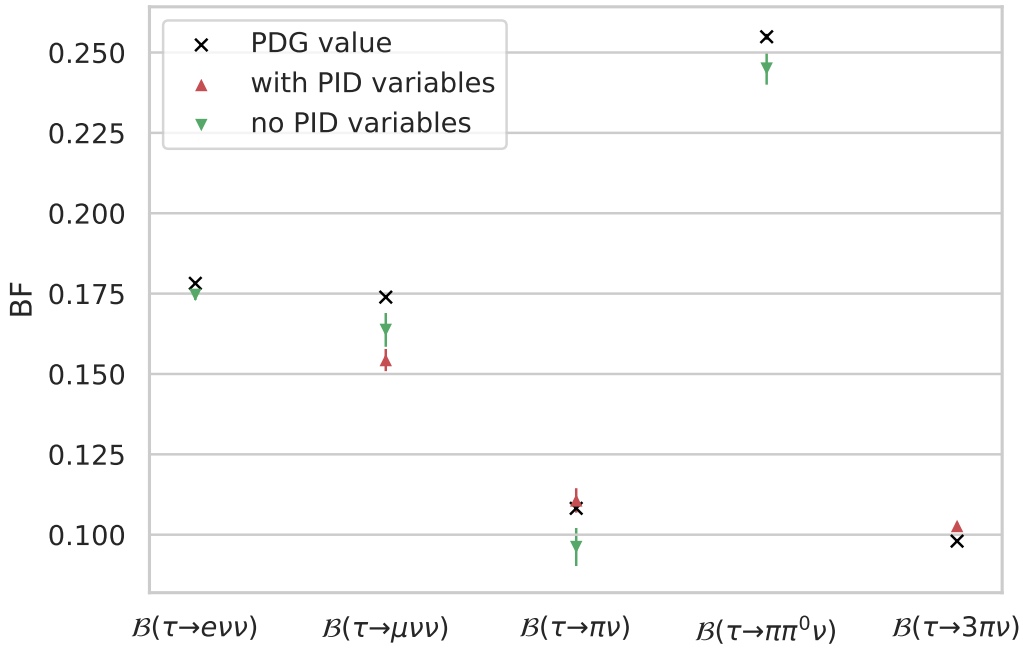

Figure 6.1: *Branching ratios.* Comparison of results of different projects with PDG values. PID variables correspond to signal enriched samples, see the relevant studies for more details.

decay mode	Calculated value	with PID cuts	PDG value [6]
$\tau \to e\nu\nu$	(17.46 ± 0.16) %		(17.82 ± 0.04) %
$\tau \to \mu\nu\nu$	(16.37 ± 0.53) %	(15.43 ± 0.35) %	(17.39 ± 0.04) %
$\tau \to \pi\nu$	(9.62 ± 0.59) %	(11.07 ± 0.38) %	(10.82 ± 0.05) %
$\tau \to \pi\pi^0\nu$	(24.5 ± 0.5) %		(25.49 ± 0.09) %
$\tau \to 3h\nu$		(10.2 ± 0.1) %	(9.8 ± 0.05) %

Table 6.1: *Branching ratios.* Branching ratios were calculated from different project working with the same data and MC. Column with PID cuts correspond to signal enriched samples, see the relevant studies for more details.

The ratios of branching ratios are shown in Table 6.2 and Figure 6.2. The $\pi\pi^0\nu$ sample is contaminated by events where π^0s were not reconstructed and so is the $\pi\nu$ sample, in the ratio of $\pi\pi^0\nu$ and $\pi\nu$ samples the π^0 reconstruction efficiency cancels out.

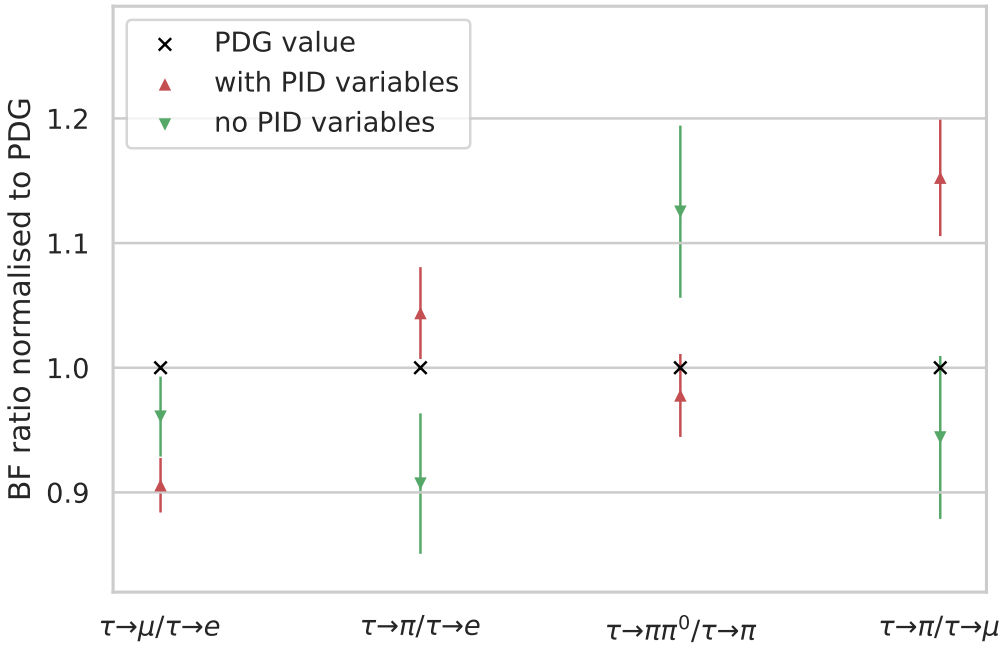

Figure 6.2: *Ratios of branching ratios.* Comparison of results of different projects with PDG values. All values in the plot are normalized to the PDG values. PID variables correspond to signal enriched samples, see the relevant studies for more details.

Ratio of BRs	Calculated value	with PID cuts	PDG value [6]
$\mathcal{BR}(\tau \to \mu\nu\nu)$ / $\mathcal{BR}(\tau \to e\nu\nu)$	0.94 ± 0.03	0.88 ± 0.02	0.976 ± 0.003
$\mathcal{BR}(\tau \to \pi\nu)$ / $\mathcal{BR}(\tau \to e\nu\nu)$	0.55 ± 0.03	0.63 ± 0.02	0.607 ± 0.003
$\mathcal{BR}(\tau \to \pi\pi^0\nu)$ / $\mathcal{BR}(\tau \to \pi\nu)$	2.55 ± 0.17	2.21 ± 0.09	2.356 ± 0.014
$\mathcal{BR}(\tau \to \pi\nu)$ / $\mathcal{BR}(\tau \to \mu\nu\nu)$	0.59 ± 0.04	0.72 ± 0.03	0.622 ± 0.003

Table 6.2: *Ratios of branching ratios.* Branching ratios were calculated from different project working with the same data and MC. Column with PID cuts correspond to signal enriched samples, see the relevant studies for more details.

7. Conclusion

The goal of this project was to measure the branching ratio of τ decay to get an insight on the detector performance.

We analyzed τ pair production data from Belle II experiment, our signal was the $\tau \to \pi\pi^0\nu$ decay channel. We simulated the signal and various backgrounds in Monte Carlo and optimized cut selections in order to get more pure sample.

The agreement between experimental data and MC was very good, smaller discrepancies are caused mainly by the π^0 reconstruction inefficiency.

We calculated the branching ratio $\mathcal{BR}(\tau \to \pi\pi^0\nu) = (24.5 \pm 0.5)\%$., only statistical uncertainties were taken into account. Despite this fact, agreement with PDG value is good.

In this note we also showed combined results from other three related project and calculated the ratio $\mathcal{BR}(\tau \to \pi\pi^0\nu)/\mathcal{BR}(\tau \to \pi\pi^0\nu)$. Here, result depends on the $\pi\nu$ channel cut selections.

This was the first study of this kind performed on this new data. It has highlighted the importance of good π^0 reconstruction and selection, which will be key to accurate measurements in these channels .

References

[1] Belle II. *Super KEKB and Belle II* [online]. [cit. 29/08/19]. https://www.belle2.org/project/super_kekb_and_belle_ii

[2] Dolezal, Zdenek, Uno, S. et al. *Belle II Technical Design Report*. arXiv:1011.0352 [physics.ins-det], 2010

[3] Joint Institute for Nuclear Research. *Electrons and Positrons Collide for the first time in the SuperKEKB Accelerator* [online]. [cit. 29/08/19]. http://www.jinr.ru/posts/electrons-and-positrons-collide-for-the-first-time-in-the-superkekb-accelerator/

[4] Particle Data Group. *Leptons - τ* [online]. [cit. 01/09/19]. http://pdglive.lbl.gov/Particle.action?node=S035&init=0

[5] Kou, Emi, Urquijo, Phillip et al. *The Belle II Physics Book*. arXiv:1808.10567 [hep-ex], 2018

[6] Particle Data Group. *2019 Review of Particle Physics* [online]. [cit. 02/09/19]. http://pdglive.lbl.gov/Viewer.action

A. Attachments

A.1. MC decay modes

MC mode	Decay channel	MC mode	Decay channel
-1	Not a tau pair event	24	$\tau^- \to \pi^-\omega\pi^0\nu$
1	$\tau^- \to e^-\nu\bar{\nu}$	25	$\tau^- \to \pi^-\pi^+\pi^-\eta\nu$
2	$\tau^- \to \mu^-\nu\bar{\nu}$	26	$\tau^- \to \pi^-\pi^0\pi^0\eta\nu$
3	$\tau^- \to \pi^-\nu$	27	$\tau^- \to K^-\eta\nu$
4	$\tau^- \to \rho^-\nu$	28	$\tau^- \to K^{*-}\eta\nu$
5	$\tau^- \to a_1^-\nu$	29	$\tau^- \to K^-\pi^+\pi^-\pi^0\nu$
6	$\tau^- \to K^-\nu$	30	$\tau^- \to K^-\pi^0\pi^0\pi^0\nu$
7	$\tau^- \to K^{*-}\nu$	31	$\tau^- \to K^0\pi^-\pi^+\pi^-\nu$
8	$\tau^- \to \pi^-\pi^+\pi^-\pi^0\nu$	32	$\tau^- \to \pi^-\bar{K}^0\pi^0\pi^0\nu$
9	$\tau^- \to \pi^-\pi^0\pi^0\pi^0\nu$	33	$\tau^- \to \pi^-K^+K^-\pi^0\nu$
10	$\tau^- \to 2\pi^-\pi^+2\pi^0\nu$	34	$\tau^- \to \pi^-K^0\bar{K}^0\pi^0\nu$
11	$\tau^- \to 3\pi^-2\pi^+\nu$	35	$\tau^- \to \pi^-\omega\pi^+\pi^-\nu$
12	$\tau^- \to 3\pi^-2\pi^+\pi^0\nu$	36	$\tau^- \to \pi^-\omega\pi^0\pi^0\nu$
13	$\tau^- \to 2\pi^-\pi^+3\pi^0\nu$	37	$\tau^- \to e^-e^-e^+\nu\bar{\nu}$
14	$\tau^- \to K^-\pi^-K^+\nu$	38	$\tau^- \to f_1\pi^-\nu$
15	$\tau^- \to K^0\pi^-K^0bar\nu$	39	$\tau^- \to K^-\omega\nu$
16	$\tau^- \to K^-K^0\pi^0\nu$	40	$\tau^- \to K^-K^0\pi^+\pi^-\nu$
17	$\tau^- \to K^-\pi^0\pi^0\nu$	41	$\tau^- \to K^-K^0\pi^0\pi^0\nu$
18	$\tau^- \to K^-\pi^-\pi^+\nu$	42	$\tau^- \to \pi^-K^+\bar{K}^0\pi^-\nu$
19	$\tau^- \to \pi^-\bar{K}^0\pi^0\nu$		
20	$\tau^- \to \eta\pi^-\pi^0\nu$		
21	$\tau^- \to \pi^-\pi^0\gamma\nu$		
22	$\tau^- \to K^-K^0\nu$		
23	$\tau^- \to \pi^-4\pi^0\nu$		

Table A.1: *MC decay modes.* Table overviews the `MCMode` variable for τ analysis. Signal mode is marked.

A.2. Cut efficiencies

cut \ sample	signal	tautau_bkg		uubar	ddbar	ssbar	ccbar
preselections	47.7 %	49.4 %		55.3 %	58.1 %	59.1 %	66.7 %
multiplicity	14.6 %	67.5 %		61.4 %	62.2 %	65.0 %	75.8 %
vis. energy	12.0 %	9.0 %		53.9 %	51.4 %	34.9 %	8.8 %
thrust	6.8 %	9.7 %		71.4 %	71.4 %	67.5 %	73.8 %
% of initial amount	36.6 %	13.5 %		2.8 %	2.2 %	3.0 %	1.9 %
	eemumu	ee	eeee	mumu	pipi	data7	data8
preselections	100 %	100 %	100 %	90.2 %	96.5 %	61.7 %	61.1 %
multiplicity	-	-	-	6.3 %	15.2 %	40.3 %	41.6 %
vis. energy	-	-	-	93.3 %	52.9 %	15.8 %	16.1 %
thrust	-	-	-	100 %	81.3 %	24.0 %	24.4 %
% of initial amount	0.0 %	0.0 %	0.0 %	0.0 %	0.2 %	14.6 %	14.4 %

Table A.2: *Cut efficiencies.* Table shows the percentage of the number of events removed by this cut for each MC component, as well as for Exp7 and Exp8 data.

A.3. Cut flow of MC plots

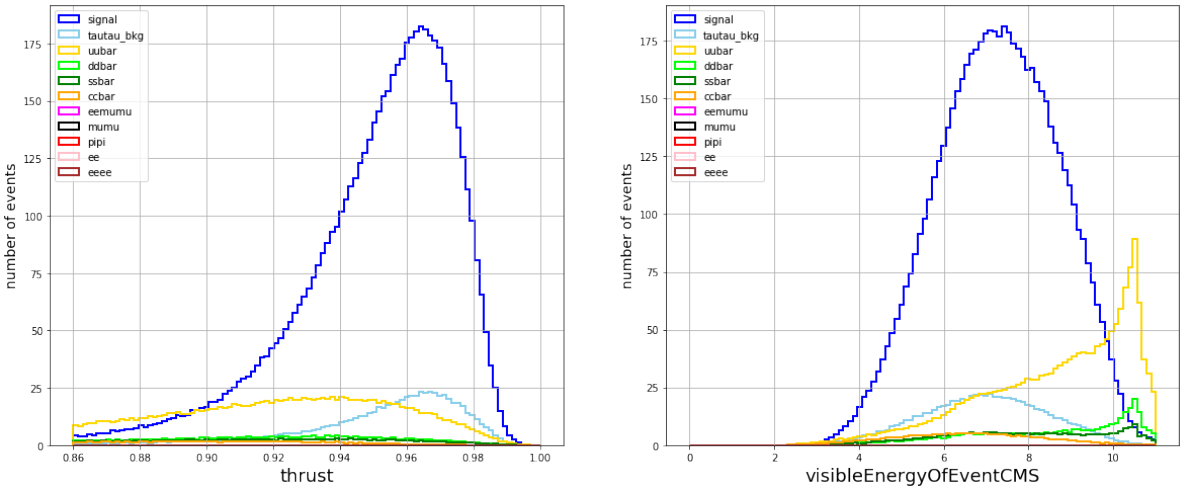

Figure A.1: *Thrust and visible energy cut flow - step 1.* Plotted after preselection and multiplicity cut. MC components are not stacked.

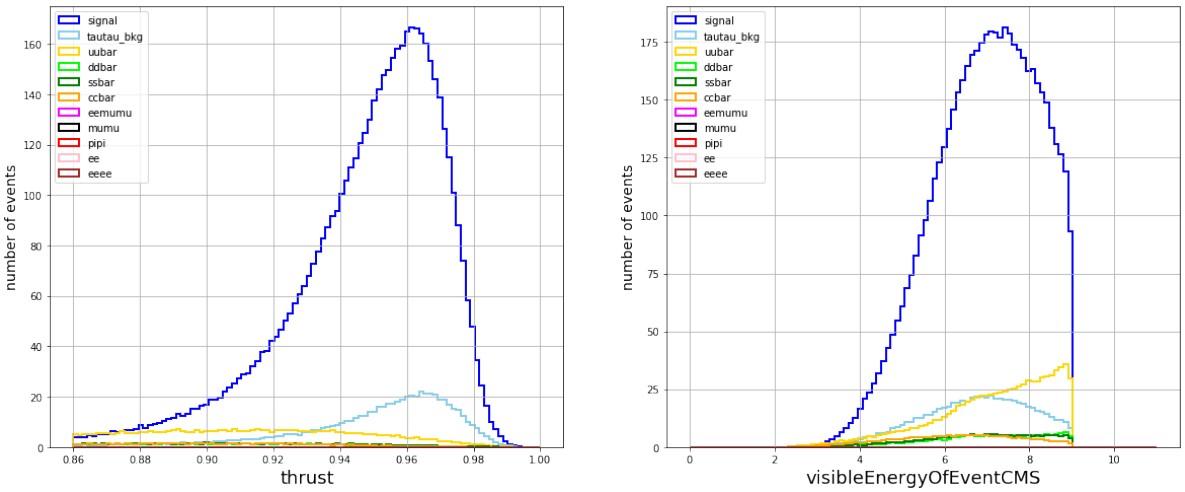

Figure A.2: *Thrust and visible energy cut flow - step 2.* Plotted after preselection, multiplicity and visible energy cut. MC components are not stacked.

A.4. Exp7 data and MC comparison plots

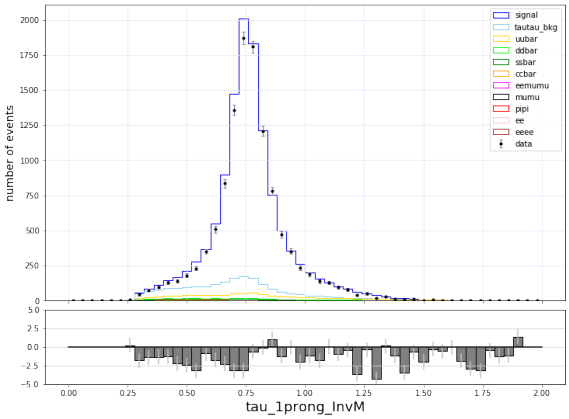

Figure A.3: *Exp7 data and MC comparison - τ 1-prong invariant mass after cuts.* MC components are stacked.

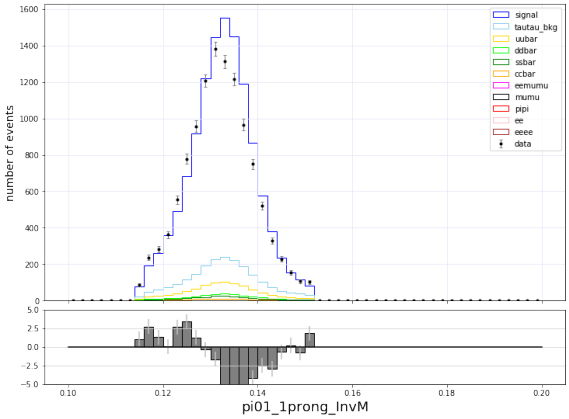

Figure A.4: *Exp7 data and MC comparison - 1-prong π^0 invariant mass after cuts.* MC components are stacked.

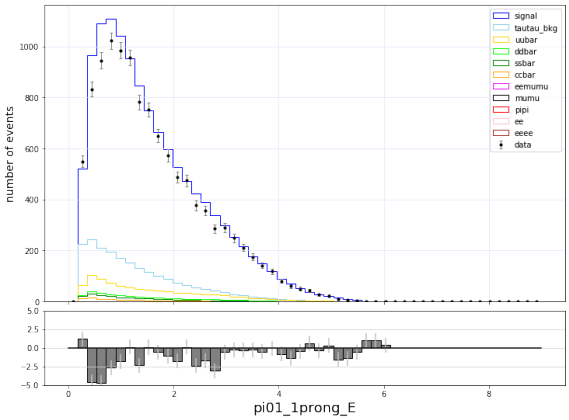

Figure A.5: *Exp7 data and MC comparison - 1-prong π^0 energy after cuts.* MC components are stacked.

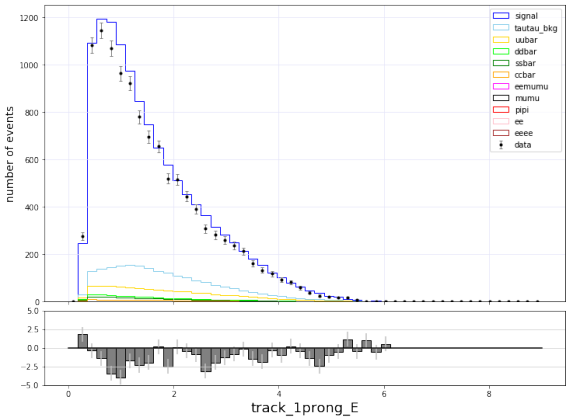

Figure A.6: *Exp7 data and MC comparison - 1-prong π energy after cuts.* MC components are stacked.